PCCP

PAPER

View Article Online
View Journal | View Issue

Cite this: *Phys. Chem. Chem. Phys.*, 2017, **19**, 19168

Nonadiabatic dynamics simulation of keto isocytosine: a comparison of dynamical performance of different electronic-structure methods†

Deping Hu,[abc] Yan Fang Liu,[abc] Andrzej L. Sobolewski[d] and Zhenggang Lan*[abc]

The nonadiabatic dynamics of keto isocytosine in the gas phase has been investigated using the on-the-fly trajectory surface hopping method based on two electronic-structure methods: SA-CASSCF and ADC(2). The results estimate an excited-state lifetime of around 1000 fs at the SA-CASSCF level, while a much shorter lifetime of 250–350 fs is obtained at the ADC(2) level. Although three conical intersections (CIs) (*Ethyl. I*, *Ethyl. II* and C=O stretching) are relevant to the nonadiabatic decay of keto isocytosine, their contributions to the nonadiabatic decay are highly dependent on the electronic-structure methods employed in the dynamics simulation. The *Ethyl. II* CI is the main channel in the dynamics simulations at the SA-CASSCF level, while the C=O stretching CI becomes dominant at the ADC(2) levels. Other high-level electronic-structure methods (MR-CISD and MS-CASPT2) are involved to benchmark our dynamics results. Through the analysis of the reaction pathways from the ground state minimum to the relevant CIs, we expect that the excited-state dynamical features obtained at the MR-CISD and MS-CASPT2 levels should be very similar to those at the SA-CASSCF level. The comparison of results obtained using different excited-state electronic-structure methods could provide guidance for further studies of similar systems.

Received 18th March 2017,
Accepted 23rd June 2017

DOI: 10.1039/c7cp01732d

rsc.li/pccp

1 Introduction

Nucleobases have received great research interest over several decades because they are basic building blocks of DNA and RNA.[1–8] After photo-excitation, they return to the ground state in an ultrafast time domain, for instance, at picosecond time scale or even less.[6–16] These ultrafast decay processes were studied intensively due to their relevance for photodamage and photostability of life.[6,8,15]

As a pyrimidine base, cytosine is particularly interesting because its different tautomers (keto, keto-imine and enol forms) display different properties in the gas phase or in biological environments.[17–19] As an important derivative of cytosine with the amino and carbonyl moieties interchanged, isocytosine is also an important compound of biological significance, because it provides an excellent prototype model to study tautomeric effects in DNA bases.[20] Moreover, isocytosine may interact with cytosine/isoguanine/guanine to form Watson–Crick or reversed Watson–Crick base pairs.[21–25] Except for its biological role, isocytosine also has numerous applications in medical sciences.[26,27]

It is well known that cytosine exhibits considerable photostability under UV irradiation due to an ultrafast decay to the molecular ground state.[6,8,14,28] Keto cytosine is the canonical form of DNA among all tautomers, and also the only one which exists in the crystalline form.[29] Thus, keto cytosine (Scheme 1) is among the most widely studied tautomers in both experimental and theoretical studies.[30–37] Several time-resolved experimental studies were conducted to investigate its excited-state dynamics at different pump wavelengths.[28,38–42] Among these studies, various time scales of excited state decay constants, from tens of femtoseconds to hundreds of picoseconds,[28,39] were obtained. Meanwhile, extensive theoretical studies were performed to examine the potential energy surfaces (PESs)[17,43–46] and excited-state dynamics[27–33,45–47] of cytosine based on different

[a] *Key Laboratory of Biobased Materials, Qingdao Institute of Bioenergy and Bioprocess Technology, Chinese Academy of Sciences, Qingdao, 266101, Shandong, People's Republic of China. E-mail: lanzg@qibebt.ac.cn; Fax: +86-532-80662778; Tel: +86-532-80662630*

[b] *The Qingdao Key Lab of Solar Energy Utilization and Energy Storage Technology, Qingdao Institute of Bioenergy and Bioprocess Technology, Chinese Academy of Sciences, Qingdao, 266101, Shandong, People's Republic of China*

[c] *University of Chinese Academy of Sciences, Beijing 100049, People's Republic of China*

[d] *Institute of Physics, Polish Academy of Sciences, PL-02668 Warsaw, Poland*

† Electronic supplementary information (ESI) available: Including active space orbitals in SA-CASSCF calculations; molecular orbitals, main electronic configurations and Cartesian coordinates of all critical geometries. See DOI: 10.1039/c7cp01732d

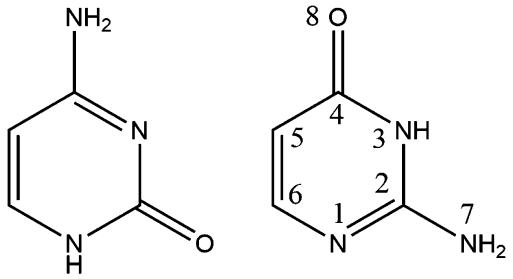

Scheme 1 Molecular structures of keto cytosine and isocytosine.

levels of electronic-structure theories, for example DFT/MRCI,[17] ROKS/BLYP,[47] CASSCF,[30,31,33–36] and OM2/MRCI.[48] Although there are some discrepancies between the results of theoretical work with respect to the excited-state lifetimes and reaction mechanisms, we nevertheless have a reasonable understanding of the nonadiabatic dynamics of cytosine.

Compared with a broad range of studies on cytosine, limited knowledge exists on the photoinduced processes in isocytosine. The early studies of this important cytosine derivative mainly focused on the studies of base-pair formation and tautomeric effects.[21–24] Besides, various experimental and theoretical studies showed that several tautomers exist for isocytosine.[49–53] The keto form (Scheme 1) is among the most widely studied ones because of its biological significance and numerous applications.[49,50] Bakalska and co-workers[54] performed an extensive theoretical study on different cytosine and isocytosine tautomers. After the location of several minimum-energy conical intersections (CIs), they proposed that the dissociative $\pi\sigma^*$ state may be responsible for the UV-induced keto to enol tautomerization reaction of isocytosine, which was reported in experimental work.[52] A similar mechanism of photoinduced dissociation–association tautomerization was discussed in previous work.[55,56] Recently, the nonadiabatic dynamics was studied by Szabla and co-workers.[57] In their work, the trajectory surface hopping (TSH) method is used to investigate the excited-state dynamics of isocytosine based on the algebraic diagrammatic construction method to the second order [ADC(2)]. Their calculations predict a very fast decay time constant ($\sim$182 fs) when the dynamics starts from higher excited singlet states. Three types of CIs (C=O stretching, ring-puckering and N–H stretching) are found, while the C=O stretching CI is the main (74%) channel responsible for the internal conversion to the ground state. They also discussed the possible role of triplet states and intersystem crossing. Although these theoretical studies provided a preliminary understanding of excited-state processes of isocytosine, we still have a very limited understanding of its nonadiabatic dynamics, particularly for the dynamics starting from the lowest excited singlet states.

In this work, the on-the-fly TSH dynamics simulations are performed for keto isocytosine using the state-averaged complete active space self-consistent field (SA-CASSCF) method. For comparison, we also show dynamics results obtained at the ADC(2) level. Contrary to previous work,[57] we consider the nonadiabatic dynamics starting from low-lying excited singlet states. Moreover, high-level electronic-calculation methods, multireference configuration interaction with single and double excitation (MR-CISD) and multi-state multiconfigurational second-order perturbation approach (MS-CASPT2), are used to benchmark the dynamics results.

In recent years, we have focused on the systematical development of nonadiabatic-dynamics theoretical methods and a simulation package JADE.[58,59] Our previous implementation allows us to perform the on-the-fly surface-hopping nonadiabatic dynamics simulation at the TDDFT and ADC(2) levels.[58–62] To simulate the nonadiabatic dynamics of isocytosine, we also added a new module to link the dynamics calculations in JADE and the CASSCF calculations in MOLPRO.[63] With the current implementation, it is possible to use our JADE code to simulate the nonadiabatic dynamics of polyatomic systems at the CASSCF level. In this sense, the current work also represents the progress of our long-term development of theoretical methods and simulation packages for nonadiabatic dynamics.

This article is organized as follows: first, the computational details are described, including the electronic-structure methods and the TSH dynamics method. Second, the results at the SA-CASSCF and ADC(2) levels, including PESs and nonadiabatic dynamics, are presented and discussed. Additional static benchmark calculation results at high levels (MR-CISD and MS-CASPT2) are also given. Finally, we summarize the whole work.

2 Computational details

The molecular structure of keto isocytosine with atomic labeling is shown in Scheme 1 and all key geometrical parameters are listed in Table 1. In this table, the double bond (C4–O8) length describing the C4=O8 stretching and the single bond (N3–H) length describing the N3–H stretching are denoted as r_a and r_b, respectively. The dihedral angles C6–N1–C2–N7 (τ_a) and C6–N3–N1–C2 (τ_b) describe the NH_2 out-of-plane and puckering of C2, respectively.

The ground-state (GS) minimum and vibrational normal modes of keto isocytosine were obtained at the B3LYP/6-31G* level of theory using the Gaussian 09 package.[64] This geometry was further used in the computation of vertical excitation energies using the SA-CASSCF[65,66] and MS-CASPT2 methods.[67] The SA-CASSCF calculations were performed using the MOLPRO[63] package, which employed different setups, *i.e.* different numbers of roots in state averaging and different active spaces as specified hereafter. Then the minimum-energy CI structures were optimized at the SA3-CASSCF(12,9) level. The MS-CASPT2 calculations were performed using the MOLCAS[68] package based on the SA-CASSCF reference wavefunction. The excited singlet states were also

Table 1 Important internal coordinates of keto isocytosine

Label	Internal coordinate	Motion
r_a	Distance C4–O8	C4=O8 stretching
r_b	Distance N3–H	N3–H stretching
τ_a	Dihedral angle C6–N1–C2–N7	NH_2 out-of-plane
τ_b	Dihedral angle C6–N3–N1–C2	Puckering of C2

computed using the ADC(2)[69,70] method implemented in TURBOMOLE[71] package. Because of the huge computational cost of the on-the-fly simulation, we employed the 6-31G* basis set in SA-CASSCF calculations and the def2-SVP basis set in the ADC(2) calculations. In the benchmark calculations, the cc-pVTZ basis set was used in the MS-CASPT2 calculations.

For benchmarking, the GS minimum and CIs were re-optimized at the MR-CISD level. We chose a similar reference space and frozen orbitals to those used in the work of Barbatti *et al.* for the treatment of cytosine,[31] to obtain a suitable description of the current system. The MR-CISD(6,5) calculations were performed based on the SA-4-CASSCF(14,10)/6-31G* results using the COLUMBUS package.[72–74]

The reaction pathways were constructed by linear interpolation between the GS minimum and relevant CIs at various levels of theories, SA-CASSCF, ADC(2), MR-CISD and MS-CASPT2.

The ultrafast nonadiabatic decay dynamics simulations of keto isocytosine were performed using the on-the-fly TSH method with Tully's fewest-switches algorithm.[75] Nuclear motion was propagated using the velocity-Verlet algorithm with a time step of 0.5 fs. In the implementation of on-the-fly surface hopping dynamics, the nuclear motion is normally integrated with a different time step than chosen for the propagation of the electronic wavefunction,[76–78] thus the electronic motion was propagated with a time step of 0.005 fs. In the electronic-structure calculations of the on-the-fly TSH simulations, both SA3-CASSCF(12,9) and ADC(2) methods were used. The potential energies and nuclear gradients were obtained directly from the QC packages [SA-CASSCF in MOLPRO and ADC(2) in TURBOMOLE]. The analytical nonadiabatic couplings at the SA-CASSCF level were obtained by calling MOLPRO directly, while the nonadiabatic couplings[79–83] were computed numerically at the ADC(2) level according to our previous implementation in the JADE package.[58,59] In our dynamics simulation, 93 and 99 trajectories were initialized from S_1 and S_2 at the SA3-CASSCF(12,9) level, and 100 and 99 trajectories started from S_1 and S_2 at the ADC(2) level, respectively.

A series of initial geometries and velocities were generated stochastically based on the Wigner distribution function[84] of the vibrational normal modes in the ground state. The decoherence effect was taken into account with the correction parameter C = 0.1 Hartree.[85] All dynamics calculations, as well as the numerical calculations of nonadiabatic couplings at the ADC(2) level, were performed with a development version of the JADE package.[58,59] A new interface module between MOLPPRO and JADE was developed to control the SA-CASSCF calculations in the dynamics run.

3 Results and discussion

3.1 SA-CASSCF results

3.1.1 Potential energy surface. The GS minimum of keto isocytosine optimized at the B3LYP/6-31G* level is shown in Fig. 1(a). Vertical excitation energies of low-lying excited states at the equilibrium geometry of keto isocytosine are given in Table 2.

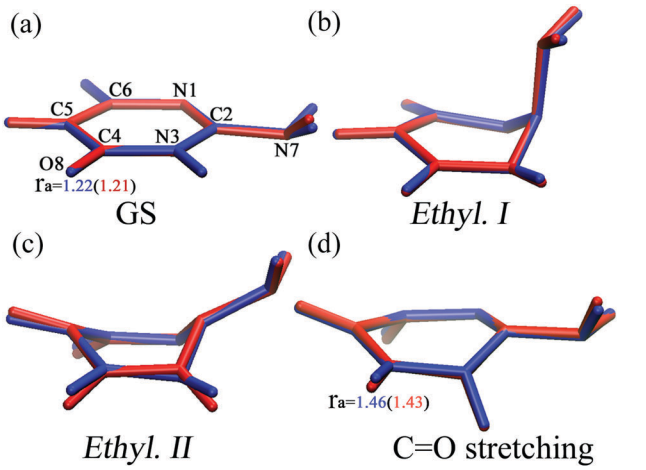

Fig. 1 Geometries of (a) ground-state (GS) minimum optimized at the B3LYP (blue) and MR-CISD (red) levels, respectively; (b–d) three conical intersections (*Ethyl. I*, *Ethyl. II* and C=O stretching) of keto isocytosine optimized at the SA3-CASSCF (blue) and MR-CISD (red) levels, respectively.

Because we only focused on the photo-induced dynamics initialized by low-energy excitations, only the lowest ππ* and nπ* excited singlet states are considered. High-lying excited states, such as the πσ* state mentioned in previous work,[54,57] are not discussed in the current work. Different root numbers in the state-averaging calculations and different active spaces were chosen in the SA-CASSCF calculations. The results show that SA-CASSCF calculations with different setups provide consistent results. Thus the SA3-CASSCF(12,9) (three states in the state average calculation with 12 electrons in 9 orbitals: four π, two n and three π*, see Fig. S1 in the ESI†) level is chosen in our dynamics simulation for computational efficiency.

The SA-CASSCF calculations predict that the lowest excited state is $n_o\pi^*$ (S_1), closely followed by a bright ππ* state (S_2) at the GS minimum. However, the ordering of these two states is different in previous ADC(2)[57] and CC2[54] calculations, as well as our own MS-CASPT2 and ADC(2) calculations (Table 2). A similar discrepancy of the excited-state order was also found in previous works on cytosine.[31,35]

Three different S_1/S_0 conical-intersection minima (CIs) are optimized at the SA-CASSCF level, as shown in Fig. 1 and Table 3.

Table 2 Vertical excitation energies (in eV) of keto isocytosine for three lowest singlet excited states. The ordering of the adiabatic S_1 and S_2 states follows the energetic order

	ππ*	$n_o\pi^*$	$n_N\pi^*$
ADC(2)/aug-cc-pVDZ[57]	4.60	4.85	5.62
CC2/aug-cc-pVDZ[54]	4.57	4.88	5.73
UV-absorption[54]	4.32	—	—
This work			
SA3-CASSCF(12,9)/6-31G*	5.34	5.03	—
SA4-CASSCF(12,9)/6-31G*	5.29	5.19	6.56
SA3-CASSCF(14,10)/6-31G*	5.35	4.96	—
SA4-CASSCF(14,10)/6-31G*	5.30	5.17	6.44
MS3-CASPT2(12,9)/cc-pVTZ	4.51	5.05	—
ADC(2)/def2-SVP	4.79	4.94	5.69

Table 3 Geometrical parameters of the ground-state (GS) minimum of keto isocytosine optimized at the B3LYP and MR-CISD (in parentheses) levels, and three conical intersections (*Ethyl. I*, *Ethyl. II* and C=O stretching) optimized at the SA-CASSCF and MR-CISD (in parentheses) levels, respectively

	r_a (Å)	r_b (Å)	τ_a (°)	τ_b (°)
GS	1.22 (1.21)	1.01 (0.99)	176.84 (176.59)	179.43 (179.50)
Ethyl. I	1.20 (1.20)	1.00 (1.00)	74.90 (74.41)	122.09 (120.02)
Ethyl. II	1.21 (1.20)	1.00 (1.00)	149.18 (156.01)	128.94 (121.08)
C=O stretching	1.46 (1.43)	1.00 (1.00)	174.95 (175.43)	164.37 (161.38)

Although both first and second S_1/S_0 CIs in Fig. 1(b) and (c) show ring puckering, they can be well distinguished by the out-of-plane motion of the NH_2 group. The NH_2 group of the first CI geometry is much more perpendicular (74.9°) to the ring plane than that of the second CI (149.2°). These two CIs were reported by two theoretical studies separately.[54,57] In addition, we noticed that similar CI geometries appear in other DNA bases, such as guanine. Previous work on guanine assigned these two types of CIs with the same geometry characters as *Ethyl. I* and *Ethyl. II* CIs[86] and thus we use the same labels here. Both *Ethyl. I* and *Ethyl. II* CIs are characterized by the crossing between the ππ* and ground states. Most importantly, the same ππ* state is involved at these two CIs, because the electronic configurations include the same frontier molecular orbitals (see Fig. S2 in the ESI†). Previous work[87] suggested that these two CI geometries are two minima on the same CI seam. However, this feature does not change our conclusion on nonadiabatic decay, because *Ethyl. I* CI always provides a very minor contribution to the dynamics simulations at both the CASSCF and ADC(2) levels (see below discussions). Also pointed out in the previous work on guanine,[86] the electronic characters of these two CIs are similar to those of the CIs in ethylene and substituted ethylene.

The third type of S_1/S_0 CI is characterized by the C4=O8 elongation [Fig. 1(d)], which was also reported in previous work.[57] This semi-planar CI displays the mixture between $n_o\pi^*$ and close shell (CS) electronic characters.

At the SA-CASSCF level, we do not optimize the N_3–H stretching CI,[57] which is related to the crossing between πσ* and CS states. In principle, this CI should only appear in the dynamics for the high-energy excitation cases,[57] thus we do not take it into account.

3.1.2 Reaction pathways. The linearly interpolated reaction pathways were constructed from the GS minimum to the S_1/S_0 CIs at the SA-CASSCF level, see Fig. 2. The energy of the ππ* state is higher than that of the $n_o\pi^*$ state in the Frank–Condon (FC) region. However, along the pathways to the *Ethyl. I* and *Ethyl. II* CIs [Fig. 2(a) and (b)], the S_2 energy decreases and the S_2/S_1 ($\pi\pi^*/n_o\pi^*$) crossing is identified near the FC region.

At the *Ethyl. I* and *Ethyl. II* CIs characterized by the CS/ππ* crossing, the energy of the S_2 state is much higher than those of the two crossing states. Although the energy of the *Ethyl. I* CI is a little lower (~0.11 eV) than that of the *Ethyl. II* CI, a steeper descent pathway exists towards the *Ethyl. II* CI. Furthermore, less distortion is needed to access the *Ethyl. II* CI, because of the lack of NH_2 out-of-plane motion. Thus we infer that the *Ethyl. II* CI channel may be preferred, which is confirmed by the dynamics simulation. Along the C=O stretching motion, the S_2 and S_1 states do not cross and the S_1/S_0 CI (mixed CS/$n_o\pi^*$) is much higher than other two S_1/S_0 CIs. Thus the C=O stretching channel should play a minor role based on the SA-CASSCF calculations, consistent with our dynamics study.

3.1.3 Nonadiabatic dynamics. TSH dynamics simulations were performed at the SA-CASSCF level for keto isocytosine. Although two lowest excited adiabatic states (S_1 and S_2) display single electronic configuration ($n_o\pi^*$ or ππ*) at the S_0 minimum, the geometrical distortion induces the significant mixture of electronic characters due to the small energy gap of the involved excited states. The clear assignment of electronic characters for each adiabatic state becomes impossible for a large number of initially sampled geometries in surface hopping dynamics. Thus we study the dynamics starting from both S_1 and S_2 states. The time-dependent occupations of electronic states are shown in Fig. 3(a) and (b).

When the trajectories are initially put into the S_2 state, as shown in Fig. 3(a), about 70% trajectories jump to S_1 within 10 fs and no population remains in the S_2 state after 100 fs. Afterwards, the occupation of the S_0 state starts to increase with

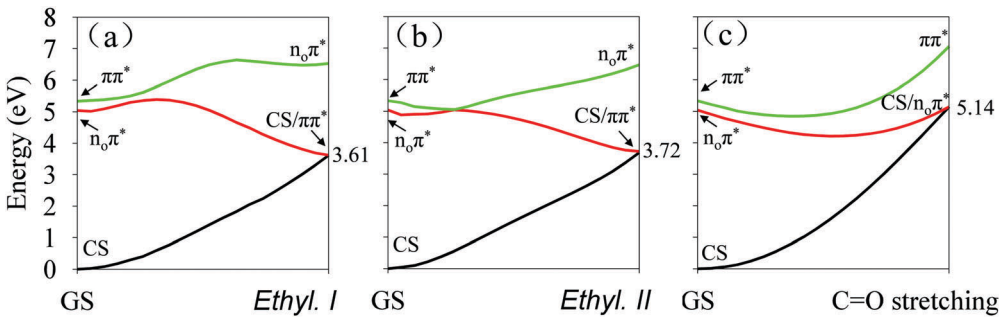

Fig. 2 Linear interpolated reaction pathways from the ground-state (GS) minimum to different S_0/S_1 CIs at the SA-CASSCF level: (a) *Ethyl. I* CI; (b) *Ethyl. II* CI; (c) C=O stretching CI. The GS minimum and the CIs are optimized at the SA-CASSCF level. The energies of CIs (in eV) are given on the right sides of the figures.

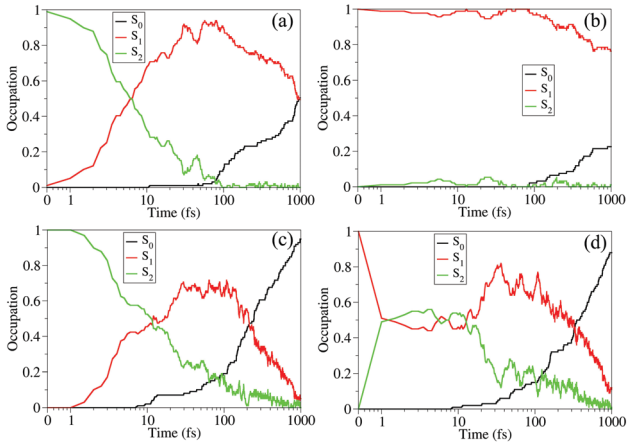

Fig. 3 Time-dependent average fractional occupations of adiabatic electronic states for nonadiabatic dynamics: (a) initiated from S_2 ($\pi\pi^*$ state at S_0 minimum-energy geometry) at the SA-CASSCF level; (b) initiated from S_1 ($n_o\pi^*$ state at S_0 minimum-energy geometry) at the SA-CASSCF level; (c) initiated from S_2 ($n_o\pi^*$ state at S_0 minimum-energy geometry) at the ADC(2) level; (d) initiated from S_1 ($\pi\pi^*$ state at S_0 minimum-energy geometry) at the ADC(2) level.

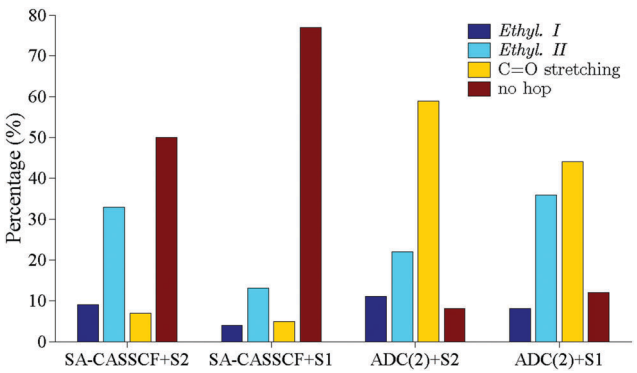

Fig. 4 Distributions of trajectories toward different reaction channels. "θ + γ" denotes that dynamics is simulated at the "θ" level [θ = SA-CASSCF, ADC(2)] and is initiated from the "γ" state (γ = S_1 or S_2).

the decrease of the occupation of the S_1 state. About 50% of the trajectories jump back to the S_0 state within ~1 ps. Fig. 3(b) shows the dynamics results initialized from the S_1 state. The $S_1 \rightarrow S_0$ nonadiabatic decay becomes slower and only 20% of the trajectories jump back to the ground state S_0 within 1 ps, and the S_2 state plays a very minor role in this case.

The distributions of trajectories towards different reaction channels are constructed in Fig. 4.

At the SA-CASSCF level, the internal conversion back to the ground state becomes less efficient when trajectories are initiated from the S_1 state with respect to the case from the S_2 state. The main reaction channel, in contrast, is not significantly dependent on the initial preparation. For both initial conditions, the *Ethyl. II* CI channel is important and other channels provide rather minor contributions. This observation is consistent with the profile of the reaction pathway in Fig. 2. It is very clear that the energy of the *Ethyl. II* CI is much lower than that of the C=O stretching CI. On the other hand, much less distortion is required to access the *Ethyl. II* CI with respect to the intramolecular motion responsible for the pathway to the *Ethyl. I* CI. Thus the *Ethyl. II* CI channel is always dominant in the decay dynamics within the simulation time (<1 ps), no matter whether the initial state is S_1 or S_2.

3.2 ADC(2) results

TSH nonadiabatic dynamics simulations were also performed at the ADC(2) level. The S_1 and S_2 states were chosen as the initial states. The vertical excited state energies (S_1, 4.79 eV, S_2, 4.94 eV in Table 2) are consistent with previous work at the ADC(2)/aug-cc-pVDZ[57] and CC2/aug-cc-pVDZ[54] levels. The time-dependent average fractional occupations of electronic states are shown in Fig. 3(c) and (d). When trajectories initially start from the S_2 state, the S_1 occupation increases very quickly in early 10 fs. After 100 fs, the occupation of the S_0 state increases significantly and reaches to 50% at about 250 fs. At the end of simulation at ~1 ps, about 95% of the trajectories decay to the ground state. When the trajectories start from the S_1 state, the S_2 state is quickly populated in the very beginning of the dynamics simulation. After 10 fs, the overall evolutions of electronic occupations are very similar to the dynamics initialized from the S_2 state, and 50% of the trajectories hop to the S_0 state at 350 fs. At the end of simulation at ~1 ps, about 88% of the trajectories decay to the ground state.

The S_1–S_2 energy gap at the ADC(2) level is smaller than that at the CASSCF level in the FC region. Due to the strong S_1–S_2 interaction, both states become populated in the early stage of the dynamics at the ADC(2) level (Fig. 3) even if the dynamics starts from the S_1 state. The internal conversion back to the ground state takes place more quickly at the ADC(2) level (250 fs from S_2 state, 350 fs from S_1 state) than the same process obtained at the SA-CASSCF level (>1000 fs). Compared with previous work on the nonadiabatic dynamics of keto isocytosine at the ADC(2) level, we notice that the internal conversion to the ground state may become much faster (~182 fs) if the trajectories start from higher excited states.[57]

Three reaction channels were also found at the ADC(2) level, as shown in Fig. 4. In addition to different lifetimes, the dynamics at the ADC(2) level also provides different reaction channels, compared to the SA-CASSCF results. The C=O stretching CI, instead of *Ethyl I/II* CIs, now becomes the main channel (53% from S_1, 64% from S_2 up to 1 ps) at the ADC(2) level. Previous dynamical simulations at the ADC(2) level also suggested that the C=O stretching CI plays an dominant role in the nonadiabatic dynamics starting from higher excited states,[57] pointing out that 74% of the trajectories hop to the ground state *via* the C=O stretching CI. Thus we may conclude that the dynamics at the ADC(2) level always prefers the C=O stretching CI, while this CI becomes even more dominant when the dynamics starts from the higher excited state.

3.3 Benchmark results

To explain the difference of the excited-state lifetimes and reaction channels between dynamics simulation results at the SA-CASSCF and ADC(2) levels, other high-level excited-state

methods (MR-CISD and MS-CASPT2) were used for benchmarking. We firstly re-optimized all relevant structures (GS minimum and CIs) at the MR-CISD level, as shown in Fig. 1. Based on these geometries at the MR-CISD level, we constructed the reaction pathways at four different levels of theories [SA-CASSCF, ADC(2), MR-CISD and MS-CASPT2], as shown in Fig. 5.

The GS minimum and relevant CI structures optimized at the MR-CISD level are very similar to those optimized at the SA-CASSCF level at first glance in Fig. 1. Thus, the profile of the SA-CASSCF-computed reaction pathways (Fig. 5) remains almost unchanged, when the SA-CASSCF-optimized structures are replaced by the MR-CISD-optimized structures. However, some discrepancies do exist when we carefully check the geometry parameters in Table 3. As a result, the SA-CASSCF calculations provide visible energy gaps at the MR-CISD-optimized *Ethyl. I* and *Ethyl. II* structures of CIs, see Fig. 5(a) and (b).

For SA-CASSCF-computed reaction pathways, S_1 and S_2 states are $n_o\pi^*$ and $\pi\pi^*$ at the FC point, respectively. When the system moves along the reaction pathways towards to the *Ethyl. I* and *Ethyl. II* CIs, we first see the S_2/S_1 crossing and they switch the electronic characters. Then the PESs towards *Ethyl. I* and *Ethyl. II* CIs provide descent pathways to these CIs. Although the pathway relevant to the C=O stretching CI shows the strong decay curve in the FC region, the energy of this CI is much higher than other two CIs. Thus the C=O stretching channel is not important in the dynamics at the SA-CASSCF level. As discussed in the previous section, the *Ethyl. II* CI requires much less geometry distortion, and thus this channel is dominant.

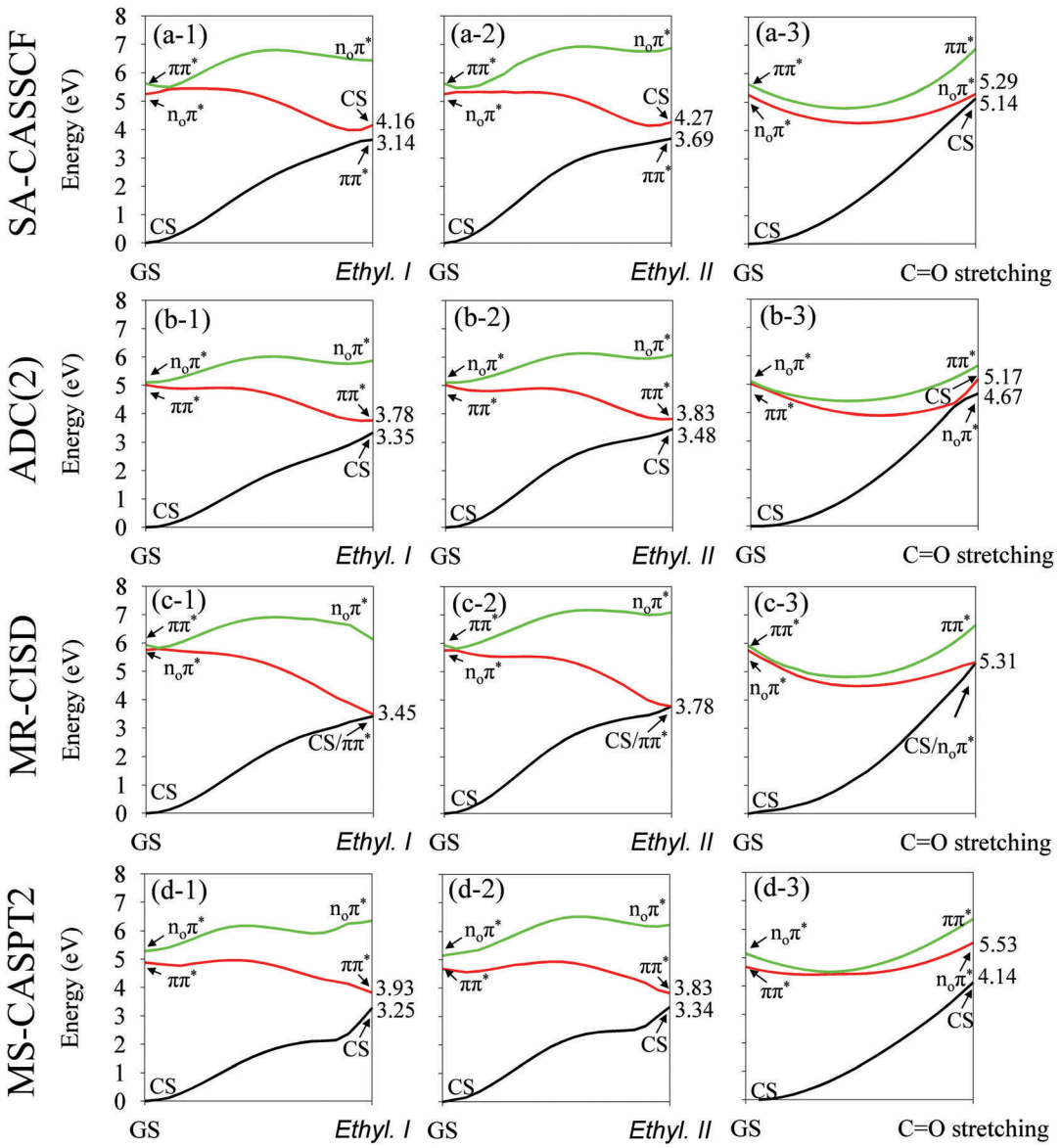

Fig. 5 Reaction pathways (linearly interpolated) from the ground-state (GS) minimum to (1) *Ethyl. I*; (2) *Ethyl. II*; (3) C=O stretching CIs, at (a) SA-CASSCF; (b) ADC(2); (c) MR-CISD; (d) MS-CASPT2 level, respectively. All GS minimum and CIs are optimized at the MR-CISD level. The energies of CIs (in eV) are given on the right sides of the figures.

Quite different pathways are obtained at the ADC(2) level [Fig. 5(b)]. The ordering of electronic characters of two low-lying excited singlet states becomes different with respect to the SA-CASSCF results. Most importantly, the C=O stretching CI is at very low energy (~4.4 eV) domain compared to the same CI at the SA-CASSCF level (~5.2 eV). Since a steeper descent reaction pathway exists towards the C=O stretching channel, this CI becomes more important for dynamical evolution at the ADC(2) level. At the same time, the *Ethyl I/II* CIs still play visible roles due to their low energies (<3.8 eV). Also due to less geometry distortion, the *Ethyl. II* CI is more important than the *Ethyl. I* CI.

The MR-CISD-computed reaction pathways [Fig. 5(c)] are very similar to the SA-CASSCF-computed ones. Thus, we expect that these two methods should provide very similar nonadiabatic dynamics and reaction mechanisms. The only minor difference is that the energy of the C=O stretching CI is slightly lower than the energy of low-lying excited states in the FC region at the MR-CISD level. Thus, we expect that such C=O stretching CI may become accessible at the MR-CISD level.

At the ADC(2) level, the C=O stretching CI lies at very low energy and thus this channel becomes very important for radiationless decay. This finding is consistent with previous theoretical studies.[57] As discussed therein, the underestimation of the CI energy may be due to the inability of ADC(2) to describe the multi-reference character of the involved electronic states.[88,89]

At the C=O strength CI the C=O bond length is around 1.46 Å at the SA-CASSCF level, while the same bond distance becomes shorter by ~1.40 Å (estimated by checking Fig. 5) at the ADC(2) level. In the early stage of dynamics, both levels of theory provide strong C=O bond stretching motion, see Fig. S3 in the ESI.† This reflects the strong gradient along the C=O bond elongation direction in the Frank–Condon region. At the ADC(2) level, the system easily accesses the C=O stretching CI in the early stage of dynamics (Fig. S3 in ESI†). Thus many trajectories decay *via* this channel and the fast nonadiabatic dynamics is observed. Although the C=O stretching motion in the early stage of dynamics displays the similar oscillation amplitude at the CASSCF level, the C=O bond distance is still not long enough to reach the C=O stretching CI during these oscillations (Fig. S3 in ESI†). Thus the C=O stretching CI channel is not the major channel at the SA-CASSCF level. The trajectories have to stay in the S_1 state for a while. After a few periods of C=O bond stretching oscillations, the strong ring distortion starts to play a role and the system decays *via* the *Ethyl. I/II* channels. Because the ring distortion involves larger motion than the C=O stretching motion, the nonadiabatic decay becomes significantly slower at the SA-CASSCF level.

Finally, we also constructed the reaction pathways at the MS-CASPT2 level, see Fig. 5(d). Although a few of the key features obtained at the MS-CASPT2 levels are consistent with the ADC(2) results, for instance the excited state ordering in the Frank–Condon region and the reaction pathways to the *Ethyl I* and *Ethyl II* CIs, a significant difference exists in the pathway towards the C=O stretching CI. Along this pathway, we do not see the S_0/S_1 crossing that seems to exist in the high energy domain in accordance with the profile of the pathway. Thus the C=O stretching channel may be absent at this level and the *Ethyl. I/II* pathways may be the dominant channels of the dynamics at the MS-CASPT2 level.

A short summary can be given as follows. (1) The *Ethyl. I* and *Ethyl. II* CIs are related to the CS/$\pi\pi^*$ intersection. (2) The C=O stretching CI is related to the CS/$n_o\pi^*$ intersection. (3) The *Ethyl. I* and *Ethyl. II* pathways are open at all calculation levels, and may be the main channels at the SA-CASSCF, MR-CISD and MS-CASPT2 levels. They are still accessible although they are not the main channels at the ADC(2) level. (4) The C=O stretching channel is the main pathway at the ADC(2) level. Compared with previous work, we know that this channel becomes even more important when the nonadiabatic dynamics starts from higher-lying excited states.[57] This channel may become more accessible at the MR-CISD level compared with the results at the SA-CASSCF level, while it may become irrelevant at the MS-CASPT2 level.

4 Conclusions

The photoinduced nonadiabatic decay dynamics of isocytosine was studied using on-the-fly TSH simulations including the ground state and the two lowest excited states. Different electronic-structure methods, SA-CASSCF and ADC(2), were employed in the simulations. Other high level theories, such as MR-CISD and MS-CASPT2, were used in a static manner to benchmark the TSH dynamics results obtained at the SA-CASSCF and ADC(2) levels.

Different excited-state lifetimes are found in the TSH dynamics simulation at the SA-CASSCF and ADC(2) levels. At the SA-CASSCF level the internal conversion to the ground state takes place at a time scale ~1000 fs, while the S_1 decay becomes faster at the ADC(2) level, 250 fs starting from the S_2 state and 350 fs starting from the S_2 state. At both levels, the decay dynamics features exhibit little sensitivity to the initial preparation of the S_1 or S_2 state.

Three types of S_0/S_1 CIs (*Ethyl. I*, *Ethyl. II* and C=O stretching) are found at the SA-CASSCF and MR-CISD levels. The *Ethyl. I* and *Ethyl II* CIs are related to the crossing between the $\pi\pi^*$ state and the ground state, while the C=O stretching CI is related to the crossing between the $n_o\pi^*$ state and the ground state. Similar CIs were also discussed in previous work on isocytosine.[54,57] The *Ethyl. II* CI is responsible for the main decay channel in the TSH simulation at the SA-CASSCF level. In contrast, the C=O stretching CI governs the main channel in the simulation at the ADC(2) level. Comparing our results with previous work,[57] we conclude that the higher initial state leads to a faster internal conversion back to the ground state and a higher reaction probability towards the C=O stretching CI at the ADC(2) level.

The different results of the SA-CASSCF and ADC(2) dynamics simulations are further explained by the reaction pathways from the FC point toward the CI points using four different methods [SA-CASSCF, ADC(2), MR-CISD and MS-CASPT2]. By comparing the profile of the reaction pathways and relevant

excited energies at critical geometries, such as FC geometry and CIs, we find that the reaction pathways at the SA-CASSCF level are closer to those at the MR-CISD level, in which the energies of *Ethyl. I* and *Ethyl. II* CIs are much lower than that of the C=O stretching CI. The pathway towards the *Ethyl. II CI* needs less deformation from the FC point. This explains why the *Ethyl. II* CI is the main channel at the SA-CASSCF level. We propose that similar dynamics results may be obtained at the MR-CISD level.

However, quite different reaction pathways are found at the ADC(2) level. First, a different ordering of the two low-lying excited states is found in the FC region. The *Ethyl. I* and *Ethyl. II* CIs are accessible at the ADC(2) level. However, the C=O stretching CI becomes very important, because of its significantly low energy at the ADC(2) level and the steep profile of the potential energy surface. It is well known that the ADC(2) as a single reference method may not provide the fully correct topography of the S_0/S_1 CI.[89] In addition, this work also clearly demonstrates that ADC(2) may also provide different potential energy profiles from the Frank–Condon region to relevant CIs, predicting different reaction channels. Similar features were also observed in previous works on other systems.[88,90,91] These findings may be attributed to the lack of multi-reference character of the ADC(2) method, as suggested by previous studies.[57,88,89]

Finally, the C=O stretching CI is located at very high energy at the MS-CASPT2 level. We expect the dynamics results at the MS-CASPT2 level to be similar to those at the SA-CASSCF level, although the excited-state order in the FC region at the MS-CASPT2 level is very similar to that at the ADC(2) level.

The current work mainly focuses on the comparison of the results for the internal conversion dynamics of isocytosine using different electronic-structure calculation methods. Such benchmark calculations provide valuable information on the influence of different electronic-structure methods on dynamics results. To obtain a clear comparison of the results at different levels, we focus on the internal conversion dynamics involving only low-lying singlet states. However, we also noticed that the current nonadiabatic dynamics (at the SA-CASSCF level) is rather slow and intersystem crossing to triplet states may start to play a role. Thus in future work, multi-state dynamics including both singlet and triplet states should be considered by simulation with TSH or other nonadiabatic dynamics methods.[33,36,92] These types of studies will provide a more comprehensive description of the nonadiabatic dynamics of isocytosine. Certainly, the theoretical study of other cytosine (or other DNA bases) derivatives with different dynamics methods at various electronic-structure levels should be a long-term research topic in the future.

Acknowledgements

This work was supported by NSFC Project (21673266 and 21607164), the Natural Science Foundation of Shandong Province for Distinguished Young Scholars (JQ201504) and the Doctoral Foundation of Shandong Province (BS2015SW012). The authors also thank Supercomputing Centre, Computer Network Information Center, CAS, National Supercomputing Center in Shenzhen, National Supercomputing Center in Guangzhou and the Super Computational Centre of CAS-QIBEBT for providing computational resources.

References

1 A. N. Alexandrova, J. C. Tully and G. Granucci, *J. Phys. Chem. B*, 2010, **114**, 12116–12128.
2 M. Barbatti, A. J. A. Aquino and H. Lischka, *Phys. Chem. Chem. Phys.*, 2010, **12**, 4959–4967.
3 M. Barbatti, A. J. A. Aquino, J. J. Szymczak, D. Nachtigallová, P. Hobza and H. Lischka, *Proc. Natl. Acad. Sci. U. S. A.*, 2010, **107**, 21453–21458.
4 R. Improta, F. Santoro and L. Blancafort, *Chem. Rev.*, 2016, **116**, 3540–3593.
5 D. Nachtigallová, T. Zelený, M. Ruckenbauer, T. Muller, M. Barbatti, P. Hobza and H. Lischka, *J. Am. Chem. Soc.*, 2010, **132**, 8261–8263.
6 M. Barbatti, A. C. Borin and S. Ullrich, *Photoinduced phenomena in nucleic acids I*, Springer International Publishing, 2014.
7 C. E. Crespo-Hernandez, B. Cohen, P. M. Hare and B. Kohler, *Chem. Rev.*, 2004, **104**, 1977–2019.
8 C. T. Middleton, K. de La Harpe, C. Su, Y. K. Law, C. E. Crespo-Hernandez and B. Kohler, *Annu. Rev. Phys. Chem.*, 2009, **60**, 217–239.
9 L. Blancafort, *J. Am. Chem. Soc.*, 2006, **128**, 210–219.
10 H. Chen and S. H. Li, *J. Phys. Chem. A*, 2005, **109**, 8443–8446.
11 W. C. Chung, Z. G. Lan, Y. Ohtsuki, N. Shimakura, W. Domcke and Y. Fujimura, *Phys. Chem. Chem. Phys.*, 2007, **9**, 2075–2084.
12 C. M. Marian, *J. Chem. Phys.*, 2005, **122**, 104314.
13 Y. Lu, Z. Lan and W. Thiel, in *Photoinduced Phenomena in Nucleic Acids II*, ed. M. Barbatti, A. C. Borin and S. Ullrich, Springer International Publishing, 2015, vol. 356, ch. 533, pp. 89–122.
14 K. Kleinermanns, D. Nachtigallová and M. S. de Vries, *Int. Rev. Phys. Chem.*, 2013, **32**, 308–342.
15 M. Shukla and J. Leszczynski, *Radiation induced molecular phenomena in nucleic acids: a comprehensive theoretical and experimental analysis*, Springer Science & Business Media, 2008.
16 V. I. Prokhorenko, A. Picchiotti, M. Pola, A. G. Dijkstra and R. J. D. Miller, *J. Phys. Chem. Lett.*, 2016, **7**, 4445–4450.
17 K. Tomic, J. Tatchen and C. M. Marian, *J. Phys. Chem. A*, 2005, **109**, 8410–8418.
18 S. A. Trygubenko, T. V. Bogdan, M. Rueda, M. Orozco, F. J. Luque, J. Šponer, P. Slavicek and P. Hobza, *Phys. Chem. Chem. Phys.*, 2002, **4**, 4192–4203.
19 R. Kobayashi, *J. Phys. Chem. A*, 1998, **102**, 10813–10817.
20 A. Y. Ivanov, S. G. Stepanian and L. Adamowicz, *J. Mol. Struct.*, 2012, **1025**, 92–104.
21 N. U. Zhanpeisov and J. Leszczynski, *Int. J. Quantum Chem.*, 1998, **69**, 37–47.

22 N. U. Zhanpeisov, J. Šponer and J. Leszczynski, *J. Phys. Chem. A*, 1998, **102**, 10374–10379.
23 N. U. Zhanpeisov and J. Leszczynski, *THEOCHEM*, 1999, **487**, 107–115.
24 C. Roberts, R. Bandaru and C. Switzer, *J. Am. Chem. Soc.*, 1997, **119**, 4640–4649.
25 A. L. Sobolewski, W. Domcke and C. Hattig, *Proc. Natl. Acad. Sci. U. S. A.*, 2005, **102**, 17903–17906.
26 J. H. Burchenal, K. Ciovacco, K. Kalaher, T. Otoole, R. Kiefner, M. D. Dowling, C. K. Chu, K. A. Watanabe, I. Wempen and J. J. Fox, *Cancer Res.*, 1976, **36**, 1520–1523.
27 L. M. Beauchamp, B. L. Serling, J. E. Kelsey, K. K. Biron, P. Collins, J. Selway, J. C. Lin and H. J. Schaeffer, *J. Med. Chem.*, 1988, **31**, 144–149.
28 K. Kosma, C. Schroter, E. Samoylova, I. V. Hertel and T. Schultz, *J. Am. Chem. Soc.*, 2009, **131**, 16939–16943.
29 D. L. Barker and R. E. Marsh, *Acta. Crystallogr.*, 1964, **17**, 1581–1587.
30 A. Nakayama, Y. Harabuchi, S. Yamazaki and T. Taketsugu, *Phys. Chem. Chem. Phys.*, 2013, **15**, 12322–12339.
31 M. Barbatti, A. J. A. Aquino, J. J. Szymczak, D. Nachtigallová and H. Lischka, *Phys. Chem. Chem. Phys.*, 2011, **13**, 6145–6155.
32 C. G. Triandafillou and S. Matsika, *J. Phys. Chem. A*, 2013, **117**, 12165–12174.
33 S. Mai, P. Marquetand, M. Richter, J. Gonzalez-Vazquez and L. Gonzalez, *ChemPhyschem*, 2013, **14**, 2920–2931.
34 H. R. Hudock and T. J. Martínez, *ChemPhyschem*, 2008, **9**, 2486–2490.
35 J. Gonzalez-Vazquez and L. Gonzalez, *ChemPhyschem*, 2010, **11**, 3617–3624.
36 M. Richter, P. Marquetand, J. Gonzalez-Vazquez, I. Sola and L. Gonzalez, *J. Phys. Chem. Lett.*, 2012, **3**, 3090–3095.
37 S. Blaser, M. A. Trachsel, S. Lobsiger, T. Wiedmer, H.-M. Frey and S. Leutwyler, *J. Phys. Chem. Lett.*, 2016, **7**, 752–757.
38 J. W. Ho, H. C. Yen, W. K. Chou, C. N. Weng, L. H. Cheng, H. Q. Shi, S. H. Lai and P. Y. Cheng, *J. Phys. Chem. A*, 2011, **115**, 8406–8418.
39 S. Ullrich, T. Schultz, M. Z. Zgierski and A. Stolow, *Phys. Chem. Chem. Phys.*, 2004, **6**, 2796–2801.
40 C. Canuel, M. Mons, F. Piuzzi, B. Tardivel, I. Dimicoli and M. Elhanine, *J. Chem. Phys.*, 2005, **122**, 074316.
41 M. Kotur, T. C. Weinacht, C. Y. Zhou and S. Matsika, *IEEE J. Sel. Top. Quantum Electron.*, 2012, **18**, 187–194.
42 H. Kang, K. T. Lee, B. Jung, Y. J. Ko and S. K. Kim, *J. Am. Chem. Soc.*, 2002, **124**, 12958–12959.
43 T. Fleig, S. Knecht and C. Hättig, *J. Phys. Chem. A*, 2007, **111**, 5482–5491.
44 M. K. Shukla and J. Leszczynski, *J. Comput. Chem.*, 2004, **25**, 768–778.
45 M. R. Silvajunior, M. Schreiber, S. P. A. Sauer and W. Thiel, *J. Chem. Phys.*, 2008, **129**, 104103.
46 P. G. Szalay, T. Watson, A. Perera, V. F. Lotrich and R. J. Bartlett, *J. Phys. Chem. A*, 2012, **116**, 6702–6710.
47 N. L. Doltsinis, P. R. Markwick, H. Nieber and H. Langer, *Radiation induced molecular phenomena in nucleic acids*, Springer, 2008, pp. 265–299.
48 Z. Lan, E. Fabiano and W. Thiel, *J. Phys. Chem. B*, 2009, **113**, 3548–3555.
49 L. Gorb, Y. Podolyan and J. Leszczynski, *THEOCHEM*, 1999, **487**, 47–55.
50 T. K. Ha, H. J. Keller, R. Gunde and H. H. Gunthard, *J. Mol. Struct.*, 1996, **376**, 375–397.
51 J. S. Kwiatkowski and J. Leszczynski, *Int. J. Quantum Chem.*, 1997, **61**, 453–465.
52 H. Vranken, J. Smets, G. Maes, L. Lapinski, M. J. Nowak and L. Adamowicz, *Spectrochim. Acta, Part A*, 1994, **50**, 875–889.
53 M. K. Shukla and J. Leszczynski, *Int. J. Quantum Chem.*, 2000, **77**, 240–254.
54 R. I. Bakalska and V. B. Delchev, *J. Mol. Model.*, 2012, **18**, 5133–5146.
55 B. Chmura, M. F. Rode, A. L. Sobolewski, L. Lapinski and M. J. Nowak, *J. Phys. Chem. A*, 2008, **112**, 13655–13661.
56 A. L. Sobolewski, *Chem. Phys. Lett.*, 1993, **211**, 293–299.
57 R. Szabla, R. W. Gora and J. Šponer, *Phys. Chem. Chem. Phys.*, 2016, **18**, 20208–20218.
58 L. K. Du and Z. G. Lan, *J. Chem. Theory Comput.*, 2015, **11**, 1360–1374.
59 L. K. Du and Z. G. Lan, *J. Chem. Theory Comput.*, 2015, **11**, 4522–4523.
60 L. K. Du and Z. G. Lan, *Phys. Chem. Chem. Phys.*, 2016, **18**, 7641–7650.
61 J. Huang, L. K. Du, J. Wang and Z. G. Lan, *J. Phys. Chem. C*, 2015, **119**, 7578–7589.
62 J. Wang, J. Huang, L. K. Du and Z. G. Lan, *J. Phys. Chem. A*, 2015, **119**, 6937–6948.
63 H. J. Werner, P. J. Knowles, G. Knizia, F. R. Manby and M. Schütz, *et al.*, *MOLPRO, version 2012.1, a package of ab initio programs*, 2012.
64 M. J. Frisch, G. W. Trucks, H. B. Schlegel, G. E. Scuseria, M. A. Robb, J. R. Cheeseman, G. Scalmani, V. Barone, B. Mennucci, G. A. Petersson, H. Nakatsuji, M. Caricato, X. Li, H. P. Hratchian, A. F. Izmaylov, J. Bloino, G. Zheng, J. L. Sonnenberg, M. Hada, M. Ehara, K. Toyota, R. Fukuda, J. Hasegawa, M. Ishida, T. Nakajima, Y. Honda, O. Kitao, H. Nakai, T. Vreven, J. A. Montgomery Jr, J. E. Peralta, F. Ogliaro, M. J. Bearpark, J. Heyd, E. N. Brothers, K. N. Kudin, V. N. Staroverov, R. Kobayashi, J. Normand, K. Raghavachari, A. P. Rendell, J. C. Burant, S. S. Iyengar, J. Tomasi, M. Cossi, N. Rega, N. J. Millam, M. Klene, J. E. Knox, J. B. Cross, V. Bakken, C. Adamo, J. Jaramillo, R. Gomperts, R. E. Stratmann, O. Yazyev, A. J. Austin, R. Cammi, C. Pomelli, J. W. Ochterski, R. L. Martin, K. Morokuma, V. G. Zakrzewski, G. A. Voth, P. Salvador, J. J. Dannenberg, S. Dapprich, A. D. Daniels, Ö. Farkas, J. B. Foresman, J. V. Ortiz, J. Cioslowski and D. J. Fox, *Gaussian 09*, Wallingford, CT, USA, 2009.
65 P. J. Knowles and N. C. Handy, *Comput. Phys. Commun.*, 1989, **54**, 75–83.
66 H.-J. Werner and P. J. Knowles, *J. Chem. Phys.*, 1985, **82**, 5053–5063.
67 J. Finley, P. A. Malmqvist, B. O. Roos and L. Serrano-Andres, *Chem. Phys. Lett.*, 1998, **288**, 299–306.

68 F. Aquilante, J. Autschbach, R. K. Carlson, L. F. Chibotaru, M. G. Delcey, L. De Vico, I. F. Galvan, N. Ferre, L. M. Frutos, L. Gagliardi, M. Garavelli, A. Giussani, C. E. Hoyer, G. Li Manni, H. Lischka, D. X. Ma, P. A. Malmqvist, T. Muller, A. Nenov, M. Olivucci, T. B. Pedersen, D. L. Peng, F. Plasser, B. Pritchard, M. Reiher, I. Rivalta, I. Schapiro, J. Segarra-Marti, M. Stenrup, D. G. Truhlar, L. Ungur, A. Valentini, S. Vancoillie, V. Veryazov, V. P. Vysotskiy, O. Weingart, F. Zapata and R. Lindh, *J. Comput. Chem.*, 2016, **37**, 506–541.

69 A. B. Trofimov and J. Schirmer, *J. Phys. B: At., Mol. Opt. Phys.*, 1995, **28**, 2299–2324.

70 J. Schirmer, *Phys. Rev. A: At., Mol., Opt. Phys.*, 1982, **26**, 2395–2416.

71 R. Ahlrichs, M. Bar, M. Haser, H. Horn and C. Kolmel, *Chem. Phys. Lett.*, 1989, **162**, 165–169.

72 H. Lischka, R. Shepard, R. M. Pitzer, I. Shavitt, M. Dallos, T. Muller, P. G. Szalay, M. Seth, G. S. Kedziora, S. Yabushita and Z. Y. Zhang, *Phys. Chem. Chem. Phys.*, 2001, **3**, 664–673.

73 H. Lischka, T. Muller, P. G. Szalay, I. Shavitt, R. M. Pitzer and R. Shepard, *WIREs Comput. Mol. Sci.*, 2011, **1**, 191–199.

74 H. Lischka, R. Shepard, I. Shavitt, R. M. Pitzer, M. Dallos, Th. Müller, P. G. Szalay, F. B. Brown, R. Ahlrichs, H. J. Böhm, A. Chang, D. C. Comeau, R. Gdanitz, H. Dachsel, C. Ehrhardt, M. Ernzerhof, P. Höchtl, S. Irle, G. Kedziora, T. Kovar, V. Parasuk, M. J. M. Pepper, P. Scharf, H. Schiffer, M. Schindler, M. Schüler, M. Seth, E. A. Stahlberg, J.-G. Zhao, S. Yabushita, Z. Zhang, M. Barbatti, S. Matsika, M. Schuurmann, D. R. Yarkony, S. R. Brozell, E. V. Beck, J.-P. Blaudeau, M. Ruckenbauer, B. Sellner, F. Plasser and J. J. Szymczak, *COLUMBUS, an ab initio electronic structure program, release 7.0*, 2015.

75 J. C. Tully, *J. Chem. Phys.*, 1990, **93**, 1061–1071.

76 M. Barbatti, G. Granucci, M. Persico, M. Ruckenbauer, M. Vazdar, M. Eckert-Maksic and H. Lischka, *J. Photochem. Photobiol., A*, 2007, **190**, 228–240.

77 M. Barbatti, *Wires Comput. Mol. Sci.*, 2011, **1**, 620–633.

78 E. Fabiano, T. W. Keal and W. Thiel, *Chem. Phys.*, 2008, **349**, 334–347.

79 E. Tapavicza, I. Tavernelli and U. Rothlisberger, *Phys. Rev. Lett.*, 2007, **98**, 023001.

80 U. Werner, R. Mitric, T. Suzuki and V. Bonacic-Koutecky, *Chem. Phys.*, 2008, **349**, 319–324.

81 I. Tavernelli, E. Tapavicza and U. Rothlisberger, *THEOCHEM*, 2009, **914**, 22–29.

82 H. Lischka, M. Dallos, P. G. Szalay, D. R. Yarkony and R. Shepard, *J. Chem. Phys.*, 2004, **120**, 7322–7329.

83 R. Mitric, U. Werner and V. Bonacic-Koutecky, *J. Chem. Phys.*, 2008, 129.

84 E. Wigner, *Phys. Rev.*, 1932, **40**, 749–759.

85 G. Granucci and M. Persico, *J. Chem. Phys.*, 2007, **126**, 134114.

86 M. Barbatti, J. J. Szymczak, A. J. A. Aquino, D. Nachtigallová and H. Lischka, *J. Chem. Phys.*, 2011, **134**, 014304.

87 L. Serrano-Andres, M. Merchan and A. C. Borin, *J. Am. Chem. Soc.*, 2008, **130**, 2473–2484.

88 D. Tuna and W. Domcke, *Phys. Chem. Chem. Phys.*, 2016, **18**, 947–955.

89 D. Tuna, D. Lefrancois, L. Wolanski, S. Gozem, I. Schapiro, T. Andruniow, A. Dreuw and M. Olivucci, *J. Chem. Theory Comput.*, 2015, **11**, 5758–5781.

90 F. Plasser, R. Crespo-Otero, M. Pederzoli, J. Pittner, H. Lischka and M. Barbatti, *J. Chem. Theory Comput.*, 2014, **10**, 1395–1405.

91 J. Huang, L. K. Du, D. P. Hu and Z. G. Lan, *J. Comput. Chem.*, 2015, **36**, 151–163.

92 B. F. E. Curchod, C. Rauer, P. Marquetand, L. Gonzalez and T. J. Martínez, *J. Chem. Phys.*, 2016, **144**, 101102.